Tunable near-infrared plasmonic perfect absorber based on phase-change materials

Yiguo Chen,[1,2] Xiong Li,[3] Xiangang Luo,[3] Stefan A. Maier,[2] and Minghui Hong[1,*]

[1]*Department of Electrical and Computer Engineering, National University of Singapore, 4 Engineering Drive 3, 117576, Singapore*
[2]*The Blackett Laboratory, Physics Department, Imperial College London, London SW7 2AZ, UK*
[3]*State Key Laboratory of Optical Technologies on Nano-Fabrication and Micro-Engineering, Institute of Optics and Electronics, Chinese Academy of Sciences, Chengdu 610209, China*
**Corresponding author: elehmh@nus.edu.sg*

Received December 18, 2014; revised January 26, 2015; accepted January 26, 2015; posted January 28, 2015 (Doc. ID 230906); published April 6, 2015

A tunable plasmonic perfect absorber with a tuning range of ~650 nm is realized by introducing a 20 nm thick phase-change material $Ge_2Sb_2Te_5$ layer into the metal–dielectric–metal configuration. The absorption at the plasmonic resonance is kept above 0.96 across the whole tuning range. In this work we study this extraordinary optical response numerically and reveal the geometric conditions which support this phenomenon. This work shows a promising route to achieve tunable plasmonic devices for multi-band optical modulation, communication, and thermal imaging.

OCIS codes: (310.6188) Spectral properties; (250.5403) Plasmonics; (310.6628) Subwavelength structures, nanostructures; (310.4165) Multilayer design.
http://dx.doi.org/10.1364/PRJ.3.000054

1. INTRODUCTION

Noble metals, such as copper, silver, and gold, are excellent reflectors in infrared (IR) regime. By patterning such metals in nanoscale, strong absorption can be produced due to the excitation of plasmonic resonance [1–10]. Among the wide range of designs, the one-side patterned metal–insulator–metal (MIM) structures have shown absorption up to 0.99, where electromagnetic energy could be efficiently confined in the sandwiched layer [2]. This extraordinary property could be promising in a variety of applications, for instance, optical modulation, communication, and thermal imaging. Unfortunately, the optical response from this plasmonic platform is fixed, which is determined by its geometric parameters and material properties. Recently, doped semiconductors have been used to replace the insulating layer. With the tunable conductivity associated with these materials upon external electric/heat stimulus, the plasmonic resonance can be spectrally shifted [3]. However, a significant decline in absorption is observed as the resonance is tuned. Together with the limited tuning range, the drawbacks severely affect the optical performance of these devices.

Phase-change materials, such as VO_2 and $Ge_2Sb_2Te_5$ (GST), have also been demonstrated in both nonplasmonic [11,12] and plasmonic [13–16] tunable absorbers. Particularly, GST receives enormous attentions due to its nonvolatile property at room temperature and the large contrast in refractive index between its different crystallization states [17–20]. Nevertheless, the reported phase-change-material absorbers still suffer from a noticeable drop in absorption efficiency during spectral tuning. In this work, we hybrid a 20 nm thick GST layer into the perfect absorber design and demonstrate that by carefully controlling the thickness of the insulator layer and the lattice size, perfect absorption can be maintained while the resonant wavelength is shifted. The GST layer is sandwiched between the gold nanodisk arrays and the SiO_2 insulating layer, serving as a tunable dielectric environment for the nanodisk array. By varying the crystallization level of GST, the plasmonic resonance of the structure can be continuously tuned in a large range of 650 nm. The absorption is kept above 0.96 and the Q-factor of the absorption peak is maintained above 4 across the entire tuning range. This highly efficient tunable plasmonic absorber is promising in applications for multi-band optical communication and thermal imaging etc.

2. DESIGN AND SIMULATION

Figure 1 schematically shows the structure of the proposed tunable perfect absorber. The two-dimensional (2D) gold disk array is on the top of the GST thin film. A layer of SiO_2 insulating spacer is sandwiched between the GST film and the metal mirror at the bottom. The disk array is arranged in a square lattice, so that the optical response from this structure is polarization-independent. To limit the number of variables in this work, we fix the thickness of the GST layer to be 20 nm; the diameter and the height of the gold disks are 300 and 20 nm, respectively.

To analyze this plasmonic system, a numerical model was constructed by using the commercial finite-difference time-domain (FDTD) software from Lumerical Solutions. A broadband plane wave polarized in x-axis is used to excite the structure at normal incidence. Periodic boundary conditions are applied to a unit cell in x- and y-directions. The dielectric functions of gold and glass are obtained from the experimental data of [21]. The complex refractive indices

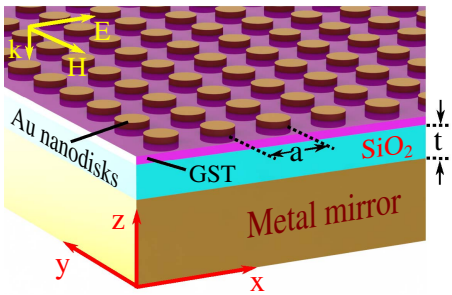

Fig. 1. Schematic drawing of the tunable perfect absorber structure. GST phase-change thin film is sandwiched between the Au disk array and the SiO_2 insulating layer. Broadband plane wave polarized in x-axis is normally incident on the Au disk array. Au disks have a diameter of 300 nm and a thickness of 20 nm. GST layer is 20 nm thick.

of GST at amorphous and crystalline phases are obtained from [22,23]. Since the crystallization process of GST is dominated by the random distributed crystalline nucleus that are formed once the temperature is above the critical point (~150°C), we assume that the GST thin film at the intermediate phases is composed of different proportions of amorphous and crystalline molecules [24]. The effective dielectric constant of GST in the intermediate phases can be estimated by the effective medium theories [25]. Based on the Lorentz–Lorenz equation, the effective permittivity of GST $\epsilon_{\text{eff}}(\lambda)$ at any crystallization level is estimated as

$$\frac{\epsilon_{\text{eff}}(\lambda)-1}{\epsilon_{\text{eff}}(\lambda)+2} = m \times \frac{\epsilon_c(\lambda)-1}{\epsilon_c(\lambda)+2} + (1-m) \times \frac{\epsilon_a(\lambda)-1}{\epsilon_a(\lambda)+2}, \quad (1)$$

where m denotes the crystallization level of the GST thin film ranging from 0 to 1; λ is the wavelength in free space; and $\epsilon_a(\lambda)$ and $\epsilon_c(\lambda)$ are the permittivities of GST in the crystalline and amorphous phases, respectively. The permittivity $\epsilon(\lambda)$ and the complex refractive index $n(\lambda)+ik(\lambda)$ are related by $\sqrt{\epsilon(\lambda)} = n(\lambda)+ik(\lambda)$.

3. RESULTS AND DISCUSSION

To begin the discussion about the tunable perfect absorber, a typical configuration with lattice constant $a = 800$ nm and the thickness of SiO_2 layer $t = 75$ nm is illustrated as an example. The evolution of the absorption spectrum as the GST crystallization level varies from 0% (amorphous phase) to 100% (crystalline phase) of this structure is shown in Fig. 2. The absorption is calculated as 1–reflection–transmission, with transmission being equal to zero because of the thick metal mirror. Two sets of absorption peaks are identified in Fig. 2,

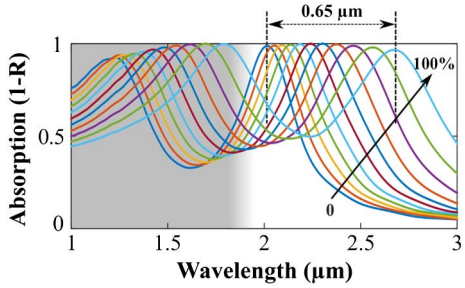

Fig. 2. Absorption spectra of the tunable perfect absorber in a variety of crystallization levels between the amorphous phase (0%) and crystalline phase (100%).

one below 2 μm shaded in gray color and the other above 2 μm. Since the crystalline GST has a larger refractive index compared to its amorphous phase, both the peaks shift significantly for a range about 650 nm as the crystallization level of GST is varied.

The nature of the two sets of absorption peaks can be revealed by studying the near-field intensity distribution at the corresponding peak positions in the spectrum. Without the loss of generality, the structure with 0% crystallized GST is investigated. Figure 3(a) shows the cross section of electric intensity in the xy plane that is 10 nm above the GST layer at the second peak ($\lambda \sim 2$ μm), illustrating a clear pattern of dipole resonance. For comparison, the electric intensity at the first peak ($\lambda \sim 1.2$ μm) with the same color range is shown in Fig. 3(a), inset. No obvious hot spots can be identified at the first peak, suggesting that the localized surface plasmon resonance (LSPR) is only excited on the gold disk at the second peak instead of the first peak.

Further analyses of the near-field electric intensity at the second peak in the xz plane reveals that the localized electric fields from the dipole resonance tunnel through the underneath GST/SiO_2 layers and extend to the mirror in the $-z$

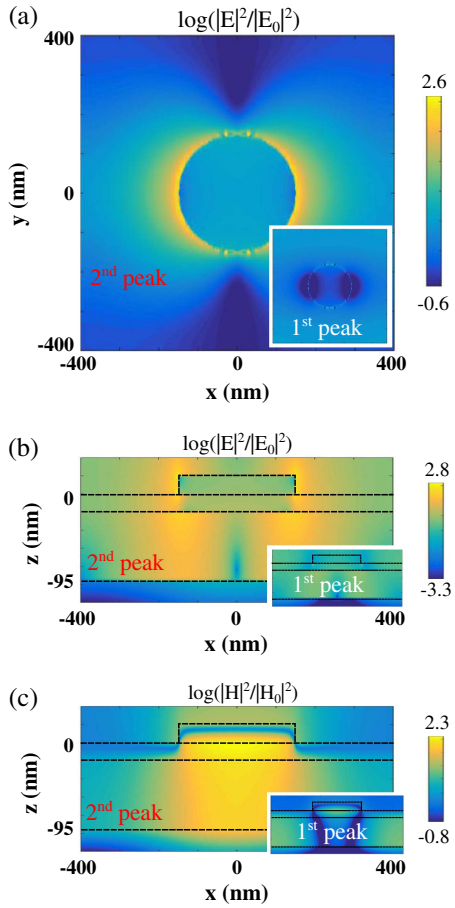

Fig. 3. (a) Enhancement of electric field intensity at the second peak in the xy cross section at 10 nm above the GST layer; (b) enhancement of electric field intensity at the second peak in the xz cross section along the diameter of the disk; (c) enhancement of magnetic field intensity at the second peak in the xz cross section along the diameter of the disk. Main panels are extracted from the structure with 0% crystallized GST. Insets, corresponding near-field enhancements at the first peak.

direction, which is shown in Fig. 3(b). The electromagnetic coupling between the Au disk and the mirror gives rise to a strongly confined magnetic resonance in the sandwiched region [Fig. 3(c)]. The combined electric and magnetic responses result in impedance matching between the free space and the demonstrated structure, which manifests as near-zero reflection or near unit absorption. For the sake of completeness, the corresponding near fields at the first peak are plotted in Figs. 3(b) and 3(c), insets. The weak localized fields in the GST/SiO_2 layers suggest that this absorption peak can be attributed to the destructive interference from the multi-layer structure.

We focus mainly on the second absorption peak because of the associated interesting properties, such as the large localized field enhancement and the tunable near-unity absorption. In Fig. 4, the absorption value at the second peak is reported as a function of the GST crystallization level, together with the corresponding quality factors (Q-factors). The maximum absorption is found to be 0.999 when GST is 60% crystallized. Although the absorption decreases at other crystallization levels, the minimum absorption is still reasonably high, which is 0.965 when GST is completely crystallized. The Q-factor, defined as the ratio between the central wavelength and the full width at half-maximum (FWHM), declines from 6 to 4 as GST is changed from the amorphous phase to the crystalline phase. This decreasing trend agrees with the expectation from the increased ohmic loss associated with the crystalline GST, which is manifested in the broadening of the absorption peak.

In the previous discussion, we investigated a specific example of the tunable perfect absorber and demonstrated its extraordinary optical response. Now, we will discuss the geometry dependence of this perfect absorption, namely varying the lattice constant a and the thickness of the SiO_2 layer t, which serves as a designing guideline for further research of this platform.

In Fig. 5, we report the 2D color maps showing the absorption at the plasmonic resonance (seco peak) as functions of the lattice constant a and the thickness of SiO_2 t for both the amorphous and crystalline phases. The range of the color bar is set in a way that any absorption value larger than 0.97 appears as bright yellow while any value below 0.95 is shown in dark blue. A band highlighting the combinations of a and t which result in more than 0.97 absorption can be clearly seen in Figs. 5(a) and 5(b) for the two GST phases. Both bands in Figs. 5(a) and 5(b) share a similar trend in that a and t increase or decrease together to maintain the "perfect" absorption. Similar conclusions were obtained in terahertz spectrum based on the circuit models from the previous studies of the perfect absorber [26,27]. However, the change of refractive

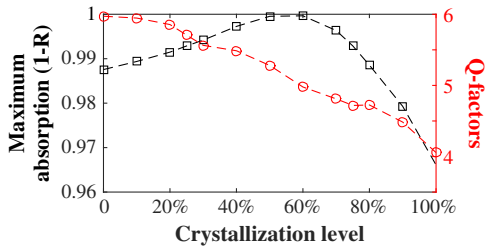

Fig. 4. Maximum absorption at the second peak and the quality factor of the second peak as functions of crystallization level.

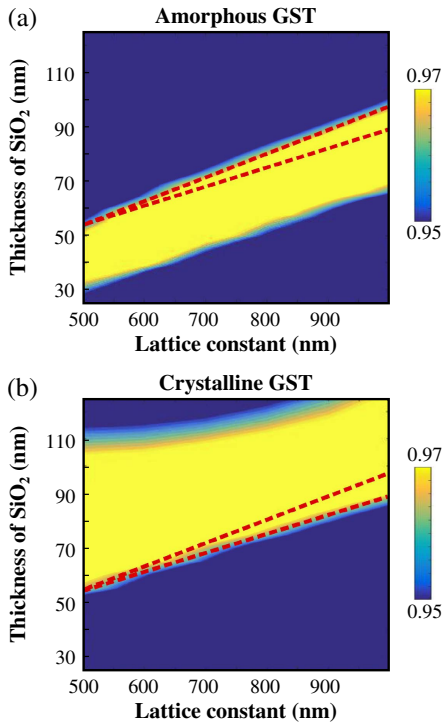

Fig. 5. 2D color maps present the absorption at the plasmonic resonance as functions of lattice constant (x-axis) and the thickness of SiO_2 layer (y-axis) for the following; (a) amorphous GST; (b) crystalline GST.

index in the GST layer from the amorphous to crystalline phase shifts the band upward to a region with larger SiO_2 thickness. Therefore, finding the suitable pairs of a and t translates into locating an overlapping region that is in yellow color from these two color maps. In this context we define the minimum acceptable absorption to be 0.96, and the red dashed lines mark the overlapping region with more than 0.96 absorption in the both phases. The example demonstrated previously with $a = 800$ nm and $t = 75$ nm falls inside the enclosed area. Indeed, the change of the refractive index of the GST layer not only shifts the resonant wavelength of the Au disks, it also modifies the impedance of the structure from the circuit-based view [26–28]. However, if the GST layer and the SiO_2 layer are regarded as a single component in the circuit model, the difference caused by the crystallization variation of the GST layer is averaged by the fixed SiO_2 layer, limiting the overall impedance change of the whole structure due to GST. This can be confirmed by the region marked by the red dashed lines in Fig. 5, where a larger thickness of SiO_2 corresponds to a wider range of lattice constant which satisfies the perfect absorption ($\geq$0.96).

4. CONCLUSIONS

A wavelength tunable perfect absorber hybridized with GST phase-change thin film has been demonstrated. By controlling the crystallization level of the 20 nm thick GST layer, the absorption peak due to the plasmonic resonance can be gradually shifted up to 650 nm. The absorption is maintained above 0.96 and the Q-factor is more than 4 across the tuning regime. Such a hybrid plasmonic system is easily implemented by current fabrication techniques. Moreover, GST has long been used in optical disks and phase-change memories; it

is well-known for the nonvolatile property at room temperature and short tuning time (~30 ns) upon external stimulus. This tunable perfect absorber can be combined with a pump laser to position the absorption peak at any specific wavelength by controlling the energy and duration of the laser pulse, achieving real-time wavelength tuning and intensity modulation. This work can lead to potential applications in multi-band optical modulation, communication, and thermal imaging.

ACKNOWLEDGEMENTS

Y. C. and M. H. acknowledge the support from the National Research Foundation, Prime Minister's Office, Singapore under its Competitive Research Program (CRP Award No. NRF-CRP10-2012-04). S. A. M. acknowledges funding from the Leverhulme trust and the EPSRC Active Plasmonics Programm. X. Li and X. Luo acknowledge funding provided by the 973 Program of China (No. 2013CBA01700) and the Chinese Natural Sciences Grant (61138002 and 61307043).

REFERENCES

1. N. I. Landy, S. Sajuyigbe, J. J. Mock, D. R. Smith, and W. J. Padilla, "Perfect metamaterial absorber," Phys. Rev. Lett. **100**, 207402 (2008).
2. N. Liu, M. Mesch, T. Weiss, M. Hentschel, and H. Giessen, "Infrared perfect absorber and its application as plasmonic sensor," Nano Lett. **10**, 2342–2348 (2010).
3. H. Zhou, F. Ding, Y. Jin, and S. He, "Terahertz metamaterial modulators based on absorption," Prog. Electromagn. Res. **119**, 449–460 (2011).
4. B. Zhang, Y. Zhao, Q. Hao, B. Kiraly, I.-C. Khoo, S. Chen, and T. J. Huang, "Polarization-independent dual-band infrared perfect absorber based on a metal-dielectric-metal elliptical nanodisk array," Opt. Express **19**, 15221–15228 (2011).
5. K. Aydin, V. E. Ferry, R. M. Briggs, and H. A. Atwater, "Broadband polarization-independent resonant light absorption using ultrathin plasmonic super absorbers," Nat. Commun. **2**, 517 (2011).
6. J. Hendrickson, J. Guo, B. Zhang, W. Buchwald, and R. Soref, "Wideband perfect light absorber at midwave infrared using multiplexed metal structures," Opt. Lett. **37**, 371–373 (2012).
7. Y. Cui, K. H. Fung, J. Xu, H. Ma, Y. Jin, S. He, and N. X. Fang, "Ultrabroadband light absorption by a sawtooth anisotropic metamaterial slab," Nano Lett. **12**, 1443–1447 (2012).
8. M. Diem, T. Koschny, and C. Soukoulis, "Wide-angle perfect absorber/thermal emitter in the terahertz regime," Phys. Rev. B **79**, 033101 (2009).
9. S. Dai, D. Zhao, Q. Li, and M. Qiu, "Double-sided polarization-independent plasmonic absorber at near-infrared region," Opt. Express **21**, 13125–13133 (2013).
10. J. Yang, F. Luo, T. S. Kao, X. Li, G. W. Ho, J. Teng, X. Luo, and M. Hong, "Design and fabrication of broadband ultralow reflectivity black Si surfaces by laser micro/nanoprocessing," Light Sci. Appl. **3**, e185 (2014).
11. M. A. Kats, D. Sharma, J. Lin, P. Genevet, R. Blanchard, Z. Yang, M. M. Qazilbash, D. N. Basov, S. Ramanathan, and F. Capasso, "Ultra-thin perfect absorber employing a tunable phase change material," Appl. Phys. Lett. **101**, 221101 (2012).
12. P. Hosseini, C. D. Wright, and H. Bhaskaran, "An optoelectronic framework enabled by low-dimensional phase-change films," Nature **511**, 206–211 (2014).
13. Q. Wen, H. Zhang, Q. Yang, Z. Chen, Y. Long, Y. Jing, Y. Lin, and P. Zhang, "A tunable hybrid metamaterial absorber based on vanadium oxide films," J. Phys. D **45**, 235106 (2012).
14. T. Cao, C. Wei, R. E. Simpson, L. Zhang, and M. J. Cryan, "Rapid phase transition of a phase-change metamaterial perfect absorber," Opt. Mater. Express **3**, 1101–1110 (2013).
15. T. Cao, L. Zhang, R. E. Simpson, and M. J. Cryan, "Mid-infrared tunable polarization-independent perfect absorber using a phase-change metamaterial," J. Opt. Soc. Am. B **30**, 1580–1585 (2013).
16. T. Cao, C. Wei, R. E. Simpson, L. Zhang, and M. J. Cryan, "Broadband polarization-independent perfect absorber using a phase-change metamaterial at visible frequencies," Sci. Rep. **4**, 3955 (2014).
17. N. Yamada, M. Otoba, K. Kawahara, N. Miyagawa, H. Ohta, N. Akahira, and T. Matsunaga, "Phase-change optical disk having a nitride interface layer," Jpn. J. Appl. Phys. **37**, 2104–2110 (1998).
18. N. Yamada, "Development of materials for third generation optical storage media," in *Phase Change Materials: Science and Applications*, S. Raoux and M. Wuttig, eds. (Springer, 2009), Chap. 10, pp. 199–226.
19. N. Yamada, "Origin, secret, and application of the ideal phase-change material GeSbTe," Phys. Status Solidi B **249**, 1837–1842 (2012).
20. Y. G. Chen, T. S. Kao, B. Ng, X. Li, X. G. Luo, B. Luk'yanchuk, S. A. Maier, and M. H. Hong, "Hybrid phase-change plasmonic crystals for active tuning of lattice resonances," Opt. Express **21**, 13691–13698 (2013).
21. E. D. Palik, *Handbook of Optical Constants of Solids*, Vol. **1** of Academic Press Handbook Series (Academic, 1985).
22. J. W. Park, S. H. Baek, T. D. Kang, H. Lee, Y. S. Kang, T. Y. Lee, D. S. Suh, K. J. Kim, C. K. Kim, Y. H. Khang, L. F. Juarez, S. Da, and S. H. Wei, "Optical properties of (GeTe, Sb_2Te^3) pseudobinary thin films studied with spectroscopic ellipsometry," Appl. Phys. Lett. **93**, 021914 (2008).
23. K. Shportko, S. Kremers, M. Woda, D. Lencer, J. Robertson, and M. Wuttig, "Resonant bonding in crystalline phase-change materials," Nature **7**, 653–658 (2008).
24. U. Russo, D. Ielmini, and A. Lacaita, "Analytical modeling of chalcogenide crystallization for PCM data-retention extrapolation," IEEE Trans. Electron Devices **54**, 2769–2777 (2007).
25. N. V. Voshchinnikov, G. Videen, and T. Henning, "Effective medium theories for irregular fluffy structures: aggregation of small particles," Appl. Opt. **46**, 4065–4072 (2007).
26. M. P. Hokmabadi, D. S. Wilbert, P. Kung, and S. M. Kim, "Design and analysis of perfect terahertz metamaterial absorber by a novel dynamic circuit model," Opt. Express **21**, 16455–16465 (2013).
27. F. Costa, S. Genovesi, A. Monorchio, and G. Manara, "A circuit-based model for the interpretation of perfect metamaterial absorbers," IEEE Trans. Antennas Propag. **61**, 1201–1209 (2013).
28. D. Zhu, M. Bosman, and J. K. W. Yang, "A circuit model for plasmonic resonators," Opt. Express **22**, 9809–9819 (2014).